High Performance Organic Mixed Ionic-Electronic Polymeric Conductor with Stability to Autoclave Sterilization

Liao, Hailiang; Savva, Achilleas; Marsh, Adam V.; Yang, Yu Ying; Faber, Hendrik; Rimmele, Martina; Sanviti, Matteo; Zhou, Renqian; Emwas, Abdul Hamid; More Authors

DOI
10.1002/anie.202416288

Publication date
2025

Document Version
Final published version

Published in
Angewandte Chemie - International Edition

How to cite: *Angew. Chem. Int. Ed.* **2025**, *64*, e202416288
doi.org/10.1002/anie.202416288

Organic Electrochemical Transistors

High Performance Organic Mixed Ionic-Electronic Polymeric Conductor with Stability to Autoclave Sterilization

*Hailiang Liao, Achilleas Savva, Adam V. Marsh, Yu-Ying Yang, Hendrik Faber, Martina Rimmele, Matteo Sanviti, Renqian Zhou, Abdul-Hamid Emwas, Jaime Martín, Thomas D. Anthopoulos, and Martin Heeney**

Abstract: We present a series of newly developed donor-acceptor (D-A) polymers designed specifically for organic electrochemical transistors (OECTs) synthesized by a straightforward route. All polymers exhibited accumulation mode behavior in OECT devices, and tuning of the donor comonomer resulted in a three-order-of-magnitude increase in transconductance. The best polymer gFBT-g2T, exhibited normalized peak transconductance ($g_{m,norm}$) of $298 \pm 10.4\ S\,cm^{-1}$ with a corresponding product of charge-carrier mobility and volumetric capacitance, μC^*, of $847\ F\,V^{-1}\,cm^{-1}\,s^{-1}$ and a μ of $5.76\ cm^2\,V^{-1}\,s^{-1}$, amongst the highest reported to date. Furthermore, gFBT-g2T exhibited exceptional temperature stability, maintaining the outstanding electrochemical performance even after undergoing a standard (autoclave) high pressure steam sterilization procedure. Steam treatment was also found to promote film porosity, with the formation of circular 200–400 nm voids. These results demonstrate the potential of gFBT-g2T in p-type accumulation mode OECTs, and pave the way for the use in implantable bioelectronics for medical applications.

Introduction

Organic electrochemical transistors (OECTs) have emerged as a forefront technology at the intersection of organic electronics and bioelectronics due to low operational voltages, biocompatibility, and ease of integration with biological systems.[1] These features offer a versatile platform for interfacing organic semiconductors with biological systems.[1a–d] Over the past few years, the development of OECTs has witnessed significant strides, propelled by advancements in materials science, device engineering, and a deeper understanding of the electrochemical processes governing their operation.[2]

The inception of OECTs was rooted in the pursuit of electronic devices that could seamlessly interface with biological entities, transcending the limitations posed by conventional rigid devices.[3] These transistors, leveraging organic semiconductors and electrolyte interfaces, provide an ideal bridge between the electronic and ionic worlds.[4] The inherent biocompatibility and soft nature of organic materials make OECTs particularly well-suited for applications ranging from bioelectronics to medical diagnostics.[5] In bioelectronics, OECTs are employed for interfacing with biological systems, such as detecting biomolecules or monitoring physiological signals.[1c] Their ability to operate in aqueous environments makes them particularly suitable for bio-sensing applications.[1b,6] Furthermore, OECTs are utilized in sensors for detecting gases, ions, and other analytes, showcasing their adaptability in chemical sensing diagnostics.[7] Their compatibility with flexible substrates enables the development of comfortable wearables and implantable devices.[1b,7b,8]

One critical aspect influencing the practical utility of OECTs in biomedical applications is their stability under

[*] H. Liao, A. V. Marsh, Y.-Y. Yang, H. Faber, R. Zhou, Prof. T. D. Anthopoulos, Prof. M. Heeney
King Abdullah University of Science and Technology (KAUST), Division of Physical Sciences & Engineering, 23955 Thuwal, Saudi Arabia
E-mail: martin.heeney@kaust.edu.sa

A. Savva
Delft University of Technology, Fac. EEMCS, Mekelweg 4, 2628 CD Delft, The Netherlands

M. Rimmele, Prof. M. Heeney
Department of Chemistry and Centre for Processable Electronics, Imperial College London, W120BZ London, United Kingdom
E-mail: m.heeney@imperial.ac.uk

M. Sanviti, Prof. J. Martín
Universidade da Coruña, Campus Industrial de Ferrol, CITENI, Campus Esteiro S/N, 15403 Ferrol, Spain

A.-H. Emwas
King Abdullah University of Science and Technology (KAUST), KAUST core lab, 23955 Thuwal, Saudi Arabia

Prof. T. D. Anthopoulos
Henry Royce Institute and Photon Science Institute, Department of Electrical and Electronic Engineering, The University of Manchester, Oxford Road, M13 9PL Manchester, United Kingdom

challenging environmental conditions, particularly at elevated temperatures.[9] For any implantable medical devices, sterilization will be essential and OECTs should ideally endure the autoclaving process without compromising their electrical performance. Achieving stability under such conditions is critical for ensuring the reliability and longevity of OECT-based technologies in the demanding field of biomedicine.[10] Thus far of the many OECT active materials reported, only poly(3,4-ethylenedioxythiophene): poly(styrenesulfonate), (PEDOT:PSS) has demonstrated stability to the standard autoclave sterilization procedure.[10–11] However, PEDOT:PSS devices operate in depletion mode, that is they are ON under zero gate bias and require a continually applied gate voltage to maintain an OFF state, which leads to high power consumption and is undesirable in many cases.[5] As such there has been much effort to develop alternative materials which can operate as accumulation mode devices,[9c,12] but to the best of our knowledge, none of these have demonstrated stability to the demanding high temperature and humidity conditions of autoclave sterilization.

In our search for higher performing accumulation mode materials for OECTs, we were drawn to donor-acceptor (D-A) conjugated polymers. These polymers are formed from the combination of donating (D) and electron-accepting (A) units, which allows for readily control of the band gap and energy levels. The use of such polymers has been highly successful in organic electronic devices such as thin film transistors, solar cells and photodetectors.[13] More recently they have been demonstrated as promising candidates for the active layer of OECTs,[14] where adjustment of the D and A monomers leads to fine-tuning of the energy levels, contributing to the improvement of electrochemical stability in OECTs by avoidance of undesirable redox side-reactions.[15] The OECT performance of D-A polymers is also strongly influenced by the nature of the sidechain, which has great impact on their electrochemical properties.[16] The amorphous and crystalline states of the polymer can be balanced by adjusting the length and nature of the glycolated side chains, further ensuring optimal ion and electron mixed conduction.[1a,12b,16]

An attractive acceptor unit for OECT polymers is benzo[*c*][1,2,5]thiadiazole (BT), which combines high electron affinity with excellent stability.[17] Copolymers of BT with extended electron-rich donor segments have already demonstrated some promise in OECT devices.[12a,18] Here we report the facile incorporation of a branched ethylene glycol sidechain onto a fluorinated BT precursor (gFBT) by nucleophilic substitution, and its subsequent copolymerisation with a range of simple donor comonomers based on thiophene (T), bithiophene (2T), thieno[3,2-*b*]thiophene (TT) and glycolated bithiophene (g2T). The branched glycol chain was choosen to ensure all polymers exhibited good solubility and the energy levels were tuned by the nature of the comonomer. OECT performance was found to be strongly influenced by the choice of comonomer, with polymers containing g2T exhibiting the best performance. Thus gFBT-g2T exhibited a three-order-of-magnitude higher normalized transconductance ($g_{m,norm} = 298 \pm 10.4\ S\,cm^{-1}$) compared to gFBT-2T, with a corresponding product of charge-carrier mobility (μ) and volumetric capacitance μC^* of $847\ F\,V^{-1}\,cm^{-1}\,s^{-1}$, the highest among all D-A polymer materials reported to date,[14b] and a μ of $5.76\ cm^2\,V^{-1}\,s^{-1}$, which is comparable with state-of-the-art materials.[19] In contrast, gFBT-3g2T with longer side chains in the donor unit, exhibited a lower $g_{m,norm}$ of $43.5 \pm 1.4\ S\,cm^{-1}$ and a μC^* of $202\ F\,V^{-1}\,cm^{-1}\,s^{-1}$. More importantly, gFBT-g2T was found to exhibit exceptionally high temperature stability, with OECTs made from gFBT-g2T maintaining excellent electrochemical performance after undergoing the standard autoclave steam sterilization procedure at 121 °C for 20 minutes. The enhanced stability of our OECT material has the potential to facilitate its application in biomedicine, opening doors for the development of more robust and reliable medical devices.

Results and Discussion

The synthesis route to the series of novel D-A polymers is illustrated in Scheme 1 and detailed in the Supporting Information. Our starting point was the readily available acceptor 4,7-dibromo-5,6-difluorobenzo[*c*][1,2,5]thiadiazole (2FBT), which was functionalized by nucleophilic substitution with a branched alcohol in good yield, using our previously reported conditions, to afford gFBT (NMR characterization data in Figures S1–S3).[20] A long branched glycol side chain was chosen to ensure sufficient polymer solubility and enhance ion penetration/transport capacity.[20–21] With the starting monomer gFBT in hand, three conjugated polymers were rapidly produced by Stille polymerization with the donor monomers (2,5-bis(trimethylstannyl)thiophene (T), 2,5-bis(trimethylstannyl)thieno[3,2-*b*]thiophene) (TT) and 5,5′-bis(trimethylstannyl)-2,2-bithiophene (2T). Based on our initial OECT device screening which identified gFBT-2T as higher performing compared to gFBT-TT and gFBT-T (see below), two further polymers were prepared by copolymerization with methoxy-substituted bithiophene (g2T) and triethyleneglycol-substituted bithiophene (3g2T) moieties to fine-tune the photophysical and electrochemical properties of the resulting polymers. Introduction of the electron donating ether groups onto the bithiophene was expected to reduce the ionisation potential of the polymers, which can help to reduce the turn-on voltage for OECT devices. Short (methoxy, g) and long (triethyleneglycol, 3 g) sidechains on the bithiophene were investigated to help decouple the role of the electron donating effect oxygen from the additional ion uptake expected from the longer 3 g sidechain. A head-to-head arrangement of the alkoxy groups, which is known to adopt a coplanar arrangement, was chosen to avoid any undesirable steric interactions with the adjacent gFBT group and facilitate backbone planarity.[22] We note that introduction of ether groups onto the T or TT co-monomers would result in their close proximity to the gFBT group with possible detrimental steric twisting.

All polymers were purified by non-solvent washing, following by extraction into chloroform. All polymers were

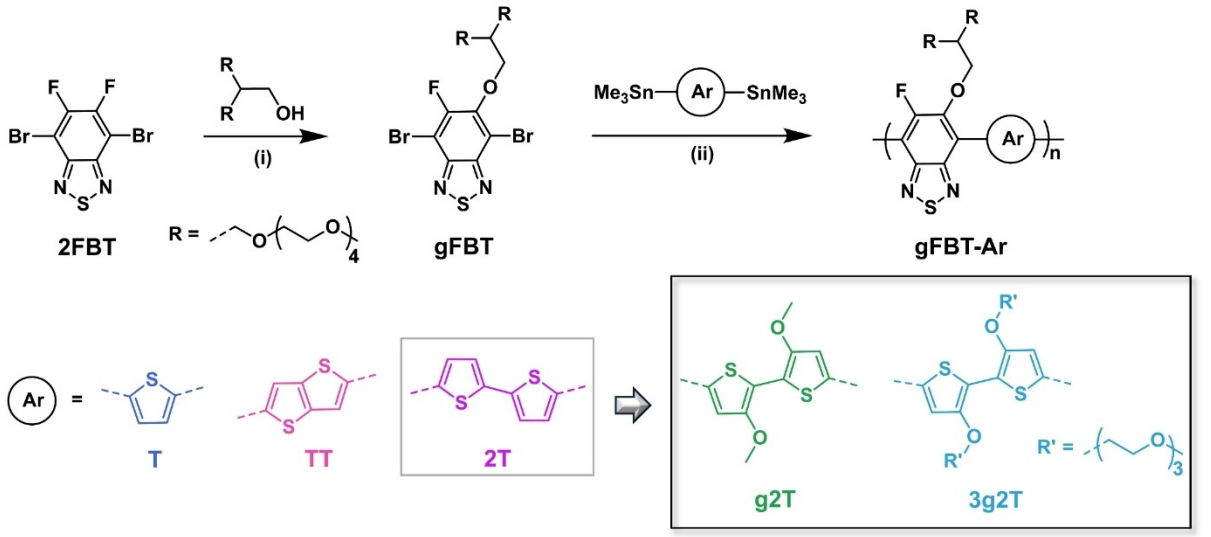

Scheme 1. Synthesis route to target monomer and polymers. Reaction conditions (i) NaH, tetrahydrofuran, reflux overnight (1.8 g, Yield = 75 %). (ii) $Pd_2(dba)_3CHCl_3$, P(o-tol)$_3$, toluene, 110 °C, 1–6 hours.

soluble in chloroform, facilitating straightforward solution processing at room temperature. ^{1}H NMR was used to confirm the polymer structures. Most of the polymers exhibited the broad, poorly resolved peaks typical of conjugated polymers (Figures S4–S8). However, gBT-3g2T exhibited a well-resolved spectrum, with all environments clearly apparent. Indeed, even the fluorine environment was observable as a singlet peak in the ^{19}F NMR spectrum (Figure S9). The improved resolution is likely related to the higher glycol sidechain density and improved solubility/reduced aggregation that this confers. Their molecular weights were determined using analytical gel permeation chromatography (GPC) with chloroform as the solvent (Table 1). Although there is some variance across the series, they are all in the high weight regime and exhibited good film-forming properties. We note that on the basis of initial OECT device data, a final preparative (Prep) GPC purification was employed for gFBT-g2T and gFBT-3g2T to reduce the Pd content in the polymers and enhance their OECT performance, with the resultant molecular weights being 126.8 kDa and 88.3 kDa.[23] All polymers demonstrated similar thermal stability, with thermal decomposition temperatures exceeding 300 °C, as determined by thermogravimetric analysis (TGA) (Figure S10).

The normalized ultraviolet–visible-near infrared (UV–Vis-NIR) absorption spectra of polymer thin films are depicted in Figure S11a and summarized in Table 1. gFBT-T, gFBT-TT, and gFBT-2T exhibited similar absorption profiles with the maximum absorption peaks ($\lambda_{max,film}$) located at 673, 687, and 682 nm, respectively. For gFBT-g2T and gFBT-3g2T, inclusion of the electron donating alkoxy groups onto the bithiophene units induced significant red-shifts in the $\lambda_{max,film}$ to 819 and 805 nm, respectively, giving them broader absorption peaks and narrower band gaps. The absorption onsets of gFBT-T, gFBT-TT, gFBT-2T, gFBT-g2T and gFBT-3g2T were found to be 742, 771, 774, 953 and 930 nm, respectively, corresponding to optical band gaps ($E_{g,opt}$) of 1.67, 1.60, 1.60, 1.30 and 1.33 eV.[24]

The ionization potential of the polymer films was measured using a photoelectron spectroscopy in air (PESA) technique, and the values used to estimate the highest occupied molecular orbital (HOMO) energy. The lowest unoccupied molecular orbital (LUMO) was calculated by adding the optical band gap, and the values are summarized in Table 1. The series of polymers undergoes a stepwise

Table 1: Optical and electronic properties.

Polymers	$\lambda_{max,\ film}$ [nm]	$\lambda_{onset,\ film}$ [nm]	$E_{g,opt}$ [eV][a]	E_{HOMO} [eV][b]	E_{LUMO} [eV][c]	M_n [kDa]/$Đ$[d]
gFBT-T	673	742	1.67	−5.22	−3.55	115.1/2.77
gFBT-TT	687	771	1.60	−5.14	−3.54	64.8/2.97
gFBT-2T	682	774	1.60	−5.04	−3.44	33.5/4.24
gFBT-g2T[e]	819	953	1.30	−4.60	−3.30	126.8/3.58
gFBT-3g2T[e]	805	930	1.33	−4.76	−3.43	88.3/1.55

[a] Derived from the absorption onset of polymer film ($E_{g,opt} = 1240/\lambda_{onset,film}$). [b] E_{HOMO} was estimated by photoelectron spectroscopy in air. Error is ±0.05 eV. [c] E_{LUMO} was calculated by the equation $E_{LUMO} = E_{HOMO} + E_{g,opt}$. [d] GPC calculated number average molecular weight (M_n) and dispersity ($Đ$) by GPC against polystyrene standards. [e] Data after preparative GPC.

change in HOMO energy levels due to variations in the donor unit's structure and side-chain modifications, changing from −5.22 eV (gFBT-T) to −4.60 eV (gFBT-g2T). Amongst the polymers, gFBT-g2T possessed the HOMO energy level closest to vacuum, making it more prone to oxidation and indicating a higher susceptibility to electrochemical doping in an aqueous electrolyte.[25] Cyclic voltammetry (CV) measurements of the polymer films in 0.1 M NaCl aqueous solution exhibited a similar trend to PESA in onset potential (Figure S11b). During the voltage cycling process, the overall current density for gFBT-T and gFBT-TT was very low, with slightly higher current density observed for gFBT-2T. The introduction of the ether side chains in the donor units resulted in significant improvements in the polymer's CV current, and notably, the shorter side chains in gFBT-g2T demonstrated even higher current density, suggesting higher ion penetration and a greater charge storage ability.[16]

Within the polymer series, gFBT-g2T and gFBT-3g2T demonstrated lower oxidation potentials and higher CV current density, which are both associated with higher OECT performance, making them the primary focus of our discussion. Spectroelectrochemical measurements were performed in 0.1 M NaCl aqueous electrolyte to investigate the polymers' doping mechanism.[12b] The electrochromic responses when the applied bias moved from −0.2 to 0.7 V under ambient conditions for gFBT-g2T and gFBT-3g2T are shown in Figure 1a and b. The same measurements on gFBT-T, gFBT-TT, and gFBT-2T showed no apparent absorption changes (Figure 1c), indicating the markedly weak ion-doping capability of these three polymers. As a comparison, Figure 1c shows the absolute changes in absorption for all five polymers, where this is clearly discernable. Returning to gFBT-g2T and gFBT-3g2T, the intensity of the π–π* absorption band gradually decreased around 800 nm with the concomitant appearance of a new absorption band from 900 to 1200 nm, assigned to polaron absorption.[26] It was observed that the polaronic absorption of gFBT-g2T emerges at 0.1 V, preceding the polaronic absorption of gFBT-3g2T (at 0.2 V). When the bias voltage was below 0.4 V, the polaronic absorption of gFBT-g2T was notably higher than that of gFBT-3g2T (Figure 1c). Subsequently, upon applying further bias to 0.6 V, the polaronic absorption intensities of both gFBT-g2T and gFBT-3g2T films became equal. However, the polaron absorption of gFBT-g2T reached saturation and remained stable, whereas gFBT-3g2T showed a minor decrease at 0.7 V. Throughout the bias voltage variation, the changes in the π–π* absorption peak intensity of gFBT-3g2T were more pronounced than those of gFBT-g2T. However, the intensity and stability of the doped polaron peaks were inferior in gFBT-3g2T, which could be attributed to its lower electrochemical redox stability during the oxidation-reduction process. This is in agreement with observations from X-ray diffraction on the thin-film, see below, which suggest greater disruption to the crystalline regions for gFBT-3g2T upon doping. Furthermore, the hydrophilicity was raised by grafting longer EG side chain, which was supported by contact angle measurements (Figure S12). The water contact angles were 72.7° and 66.6° for gFBT-g2T and gFBT-3g2T, respectively. Higher hydrophilicity can facilitate ion penetration into the film, but it is a balance since excessive swelling can disrupt crystallinity and charge transport pathways.[16]

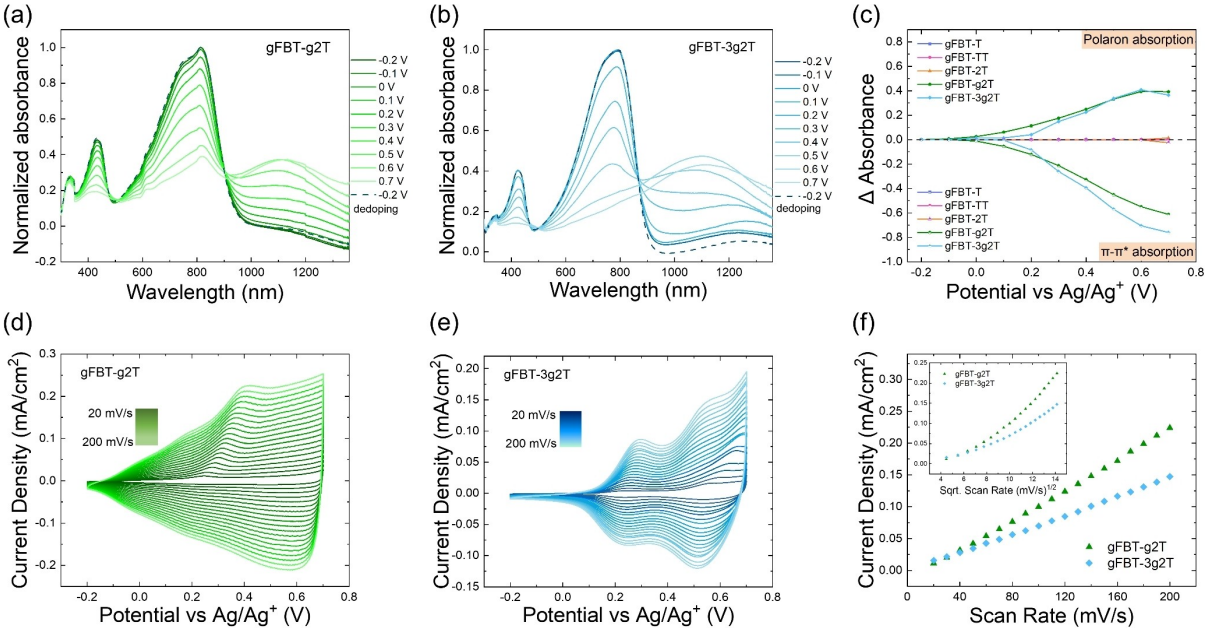

Figure 1. (a) Potential-dependent UV–Vis-NIR polymer film absorption spectra of gFBT-g2T, and (b)gFBT-3g2T. (c) Absolute changes in polaron absorption and π–π* absorption of the films versus applied bias. 20–200 mV s^{-1} scan rate dependence CV of (d) gFBT-g2T, and (e) gFBT-3g2T in 0.1 M aqueous NaCl solution. (f) Peak currents versus scan rates for gFBT-g2T and gFBT-3g2T, with the inset displaying peak currents against the square roots of scan rates.

To investigate the volumetric penetration of counterions into polymer thin films, we collected scan rate dependent CV data from −0.2 V to 0.7 V in 0.1 M NaCl aqueous electrolyte (Figure 1d–f).[18a] As shown in Figure 1f, a clear dependence of current on scan rate was observed, suggesting counterion penetration throughout the bulk of the film. However, plotting the square route of voltage against current density (Figure 1f, inset), did not follow the linear relationship observed in diffusion-controlled thin film oxidation following the Randles–Sevcik equation.[18,27] Rather, gFBT-g2T and gFBT-3g2T showed a superlinear relationship between current density and square root of scan rate, which we speculate might relate to the fluorine on the acceptor unit helping to overcome the kinetic limitations and boosting charge/discharge cycling properties.[28] Notably, gFBT-g2T and gFBT-3g2T still exhibited the same curve relationship when we increased the scan rate to 1000 mV/s (Figure S13).

OECT devices were fabricated to evaluate the mixed ionic and electronic transport characteristics of these novel D-A polymers. The output and transfer characteristics of the OECTs are shown in Figure 2 and Figure S14, and the corresponding data is summarized in Table 2. All polymers behaved as p-type accumulation mode OECTs. The OECT device data of the polymer series exhibited similar trends to the CV current. The transfer curve currents for gFBT-T and gFBT-TT were extremely low, resulting in very small values for their normalized peak transconductances ($g_{m,norm}$) of $0.021 \pm 3.5\times10^{-4}$ and $0.086 \pm 8.7\times10^{-3}$ S cm^{-1} respectively, and products of charge-carrier mobility and volumetric capacitance (μC^*) of 0.243 and 1.15 F V^{-1} cm^{-1} s^{-1}. The channel current for gFBT-2T showed a certain degree of enhancement, with higher $g_{m,norm}$ of $0.30 \pm 2.5\times10^{-2}$ S cm^{-1} and a corresponding μC^* of 4.03 F V^{-1} cm^{-1} s^{-1}. In all cases, the threshold voltage (V_{Th}, Figure S16) for the devices were all exceedingly high (−0.71, −0.67, −0.62 V), which could be attributed to the low swelling of the films, their low ionic

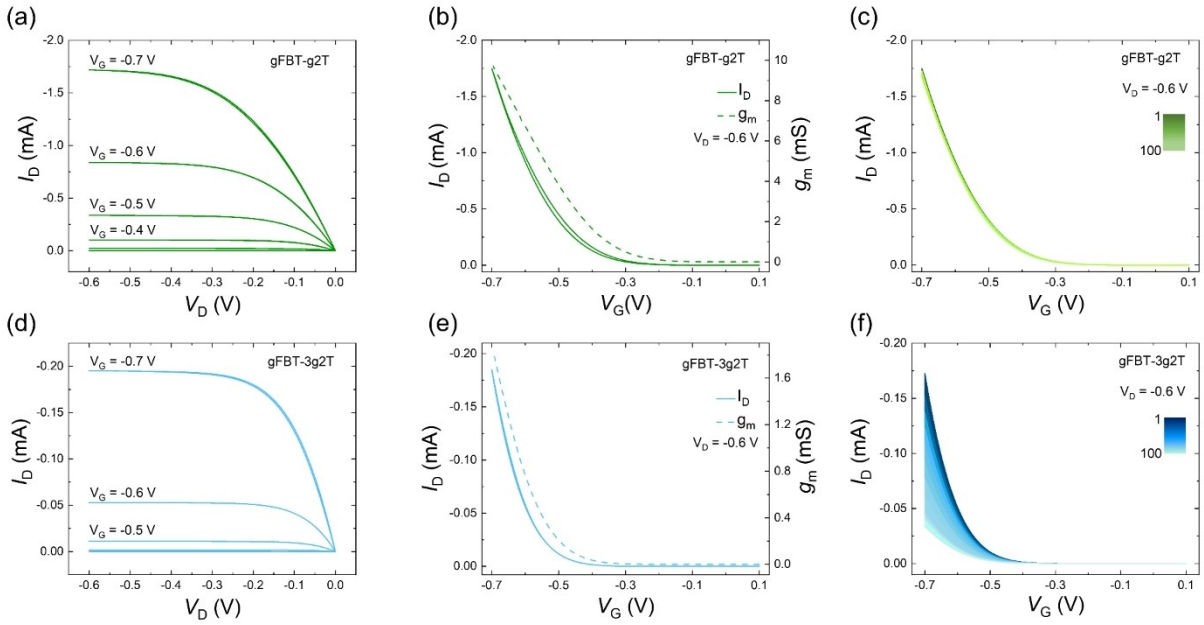

Figure 2. OECTs output curves of (a) gFBT-g2T, and (d) gFBT-3g2T at stepped V_G from 0 to −0.7 V in 0.1 V intervals. Transfer and transconductance curves of (b) gFBT-g2T, and (e) gFBT-3g2T at $V_D = -0.6$ V. (100 consecutive saturation transfer curves measured from OECT channels made of (c) gFBT-g2T, and (f) gFBT-3g2T. All OECT channels studied were 100 μm in length and 10 μm in width and biased at $V_D = -0.6$ V in a 0.1 M NaCl aqueous solution in ambient conditions.

Table 2: Summary of the characteristics of OECTs.

Polymer	d [nm]	V_{Th} [V][a]	$g_{m,norm}$ [S cm^{-1}][b]	μC^* [F V^{-1} cm^{-1} s^{-1}][c]	C^* [F cm^{-3}][d]	μ [cm^2 V^{-1} s^{-1}][e]	τ_{on} [ms]	τ_{off} [ms]
gFBT-T	28.4 ± 2.7	−0.71	$0.021 \pm 3.5\times10^{-4}$	$0.24(0.24 \pm 4) \times10^{-3}$	25 ± 2	0.0097	99	55
gFBT-TT	32.6 ± 3.1	−0.67	$0.086 \pm 8.7\times10^{-3}$	1.15(1.07 ± 0.11)	31 ± 3	0.037	102	55
gFBT-2T	28.5 ± 1.8	−0.62	$0.30 \pm 2.5\times10^{-2}$	4.03(3.81 ± 0.31)	133 ± 8	0.030	70	38
gFBT-g2T	32.9 ± 1.7	−0.33	298 ± 10.4	847 (826 ± 28.8)	147 ± 10	5.76	19	10
gFBT-3g2T	40.1 ± 4.0	−0.47	43.5 ± 1.4	202(198 ± 6.4)	292 ± 14	0.69	23	9

[a] Values determined by extrapolating the corresponding $I_D^{1/2}$–V_G plots. [b] The average transconductance values normalized by the channel geometry. [c] Maximum and average data calculated from the equation: $g_m = WdL^{-1}\mu C^*(V_{Th} - V_G)$. [d] Data deduced from EIS plots. [e] Data obtained from the μC^* and the volumetric capacitance C^*.

conductivity and high HOMO levels, necessitating a high bias voltage for film oxidation.[29]

The introduction of methoxy or glycolated side chains to the donor units, resulted in a significant improvement in device performance and a marked decrease in threshold voltage. The $g_{m,norm}$ of gFBT-g2T increased by three orders of magnitude ($298 \pm 10.4\ S\,cm^{-1}$) compared to gFBT-2T, with a corresponding μC^* of $847\ F\,V^{-1}\,cm^{-1}\,s^{-1}$, which is the highest among all D-A polymer materials reported to date, to the best of our knowledge (see Table S1). In comparison, gFBT-3g2T, with longer donor unit side chains, showed reduced performance with $g_{m,norm}$ of $43.5 \pm 1.4\ S\,cm^{-1}$, and a lower μC^* of $202\ F\,V^{-1}\,cm^{-1}\,s^{-1}$. These results are in agreement with other studies showing that longer glycolated side chains do not necessarily provide an advantage in OECT device performance.[12b,18b] Typically there is a balance between glycolated sidechains beneficially enhancing ion transport and sidechains leading to excessive film swelling during the electrochemical doping process, reducing the crystallinity of the film and consequently impacting the charge transport capability of the film.[1a,16,30] Therefore, balancing the coupled transport capabilities of ions and holes in our polymer design was crucial for optimizing OECT performance. It is worth noting that the V_{Th} of gFBT-g2T was −0.33 V, which was lower than that of gFBT-3g2T (−0.47 V) with longer donor unit glycolated side chains. The shift in the device V_{Th} for these polymers, ranging from −0.71 V to −0.33 V, is correlated with their onsets of polaronic absorption (Figure 1c), a lower potential for the transition from a neutral state to a polaronic state indicated a lower threshold voltage.[31] The device data discussed were recorded for both polymers after purification by passage through a preparative GPC, in accordance with literature reports.[23] We note that this resulted in an improvement in the maximum device current and transconductance of approximately 25 % compared to the unpurified polymers (see Figure S15).

To better understand the volumetric doping process of these polymer thin films, electrochemical impedance spectroscopy (EIS) measurements were performed to evaluate their volumetric capacitances (C*) (Figure S17, S18). gFBT-T and gFBT-TT exhibited closely similar low C^* (25 ± 2 and $31 \pm 3\ F\,cm^{-3}$) values, while gFBT-2T showed a significant increase in C^* ($133 \pm 8\ F\,cm^{-3}$). With the introduction of methoxy groups to the donor unit, the capacitance of gFBT-g2T increased modestly to $147 \pm 10\ F\,cm^{-3}$. Changing to the longer glycolated side chains of gFBT-3g2T resulted in a large increase in C^* to $292 \pm 14\ F\,cm^{-3}$, likely due to increased ion uptake. Based on the μC^* and C^* values, the charge mobilities of polymers could be calculated and summarized in Table 2. gFBT-g2T possessed the highest μ value ($5.76\ cm^2\,V^{-1}\,s^{-1}$) among these polymers, which was comparable with state-of-the-art materials.[14b,19]

The decay time constants for the ON (τ_{on}) and OFF (τ_{off}) processes were extracted by fitting the temporal response curve with the exponential decay equation $I_D(t) = I_{D,0} + A \times \exp(-t/\tau)$ (Figure S19 and S20).[21] The τ_{on}/τ_{off} values of these polymers were summarized in Table 2. The response times of devices based on gFBT-T, gFBT-TT, and gFBT-2T were relatively slow. However, after introducing glycolated side chains to the donor unit, the enhanced ion-doping capability effectively improved the response speed of the devices. The τ_{on}/τ_{off} values were estimated to be 19/10, and 23/9 ms for gFBT-g2T and gFBT-3g2T.

To investigate the stability of the materials during device operation, we conducted repetitive tests of the saturated transfer curves for gFBT-g2T and gFBT-3g2T over 100 cycles. It was observed that the transfer curve current for gFBT-g2T was nearly unchanged, with the curves after 100 cycles almost overlapping the initial transfer curve, demonstrating promising device stability. However, the current for gFBT-3g2T decreased appreciably, with the maximum current after 100 cycles being only about 20 % of the initial value, indicating poorer stability. The long-term operational stabilities of polymers were also investigated by monitoring the variation of drain current upon applying successive pulse bias (pulse length = 5 s) (Figure S21). Among the tested polymers, only gFBT-g2T exhibited good long-term operational stability with pulse bias between 0 and −0.5 V, maintaining 70 % of its maximum current after 60 minutes of 720 on-off cycles.

To further investigate the ability of gFBT-g2T to withstand the harsh sterilization conditions required for applications in the clinic, we designed a series of tests. Firstly, we explored the stability of the films of gFBT-g2T and gFBT-3g2T during extended annealing time under nitrogen conditions. Thus, OECT devices were exposed to continuous heating at 100 °C for a duration of 120 minutes within a glovebox, and the electrical characteristics of the OECTs were measured before the annealing process, at various intermediate time points during annealing and after the completion of annealing, each measurement being performed at room temperature outside the glovebox. As shown in Figure 3a, the devices of gFBT-g2T retained excellent electronic properties (as high as 99 % of the original current and transconductance) under extended annealing time. Whereas the saturation current of gFBT-3g2T dropped to 83 % after annealing for 10 minutes, and continued to decrease steadily upon extended annealing, dropping to 51 % of the initial value after 120 minutes. We further investigated the temperature response with variable temperature annealing, starting from 50 °C, with increments of 25 °C, and testing in air after annealing for 10 minutes at each temperature. Interestingly, whilst gFBT-g2T managed to maintain 98 % of the saturation current and transconductance of the initial values after annealing at 125 °C, gFBT-3g2T retained less than 25 % of these values, and showed a decrease even after annealing at 50 °C (Figure 3b). The above tests demonstrated the exceptional thermal stability of gFBT-g2T under nitrogen conditions, while the devices of gFBT-3g2T couldn't survive under high temperature conditions. Moving to ambient atmosphere, gFBT-g2T devices continued to show impressive performance, with the current and transconductance retaining 84 % of their initial values after annealing for 30 minutes (Figure 3c).

To investigate performance under typical sterilization procedures, we initially immersed devices of gFBT-g2T into boiling water at 100 °C under atmospheric pressure for half

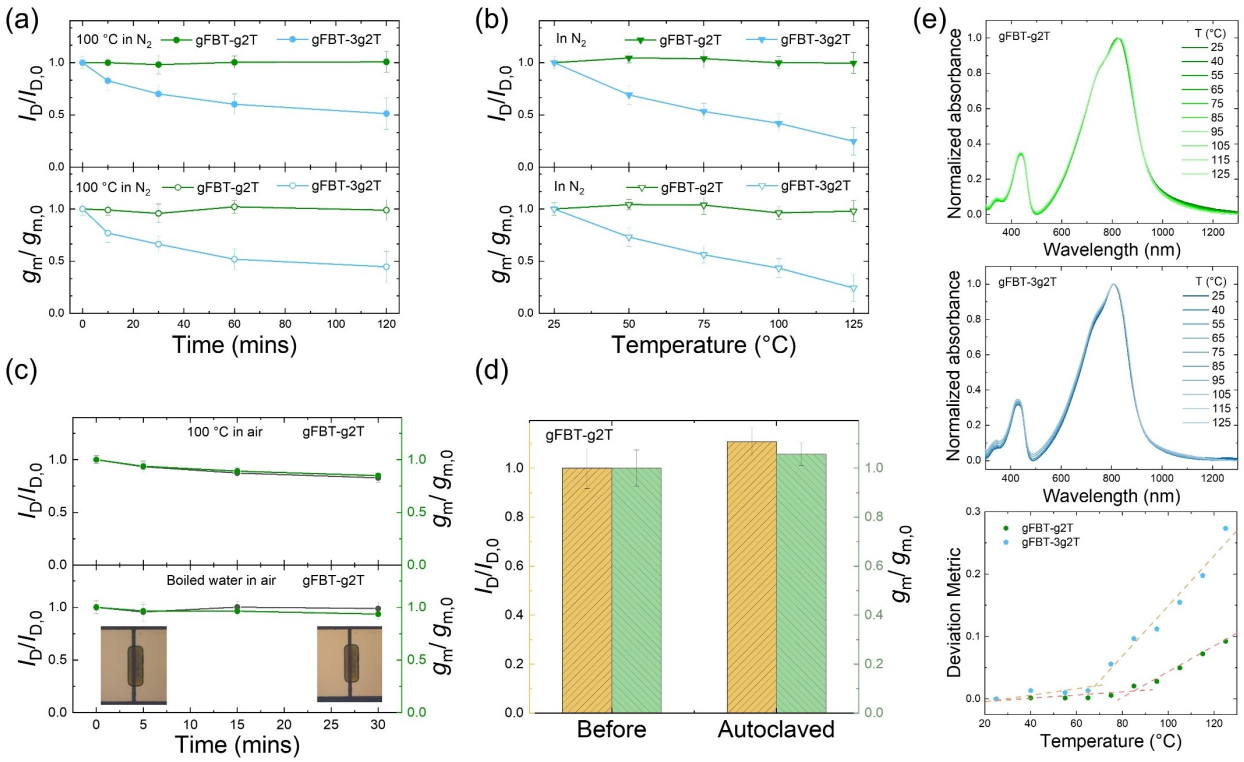

Figure 3. The stability of the saturated current and transconductance (measured from the slope of I_D vs V_g) for gFBT-g2T and gFBT-3g2T after different annealing times at 100 °C in (a) nitrogen condition, and (b) after different annealing temperatures, each temperature involving a 10 mins annealing in N_2. (c) Device stability of the saturated current and transconductance for gFBT-g2T after different annealing times exposed in air at 100 °C (upper panel) and immersed into boiling water in air (lower panel), the inset images show the optical images of the same channel before and after being immersed in boiling water for 30 minutes. (d) The stability of the saturated current and transconductance for gFBT-g2T before and after the standard autoclave sterilization. (e) Thin-film absorption spectra of gFBT-g2T (upper panel) and gFBT-3g2T (middle panel) for the annealing temperatures indicated, and evolution of the deviation metric as a function of annealing temperature (lower panel).

an hour. As shown in Figure 3c, the devices still maintained over 98 % of the initial current and 94 % of the initial transconductance. The improved performance compared to annealed films in air is possibly due to water reducing the local oxygen content, preventing oxidative degradation of the film. It is worth emphasizing that, unlike other organic based devices that required encapsulation by parylene before immersion into boiling water,[32] direct immersion of gFBT-g2T devices into boiling water did not result in the detachment of the channel film, indicating the strong adhesion of the gFBT-g2T film to glass (Figure 3c, inset images). This is likely due to the hydrogen bonding interactions of the polar and hydrophilic sidechains of gFBT-g2T with the surface silanols present on the glass surface. Strong adhesion of the conjugated polymer to the underlying substrate is also a critical parameter for long-lived recordings in biological settings.[33]

Since gFBT-g2T maintained film integrity and stable device current after soaking in boiling water, we finally investigated the standard sterilization procedure in an autoclave, exposing devices to pressurized steam at a temperature of 121 °C for 20 minutes.[10] Remarkably the devices of gFBT-g2T not only survived, but also exhibited a slight increase in the channel current and transconductance (Figure 3d), which might imply that the film microstructure of gFBT-g2T underwent an additional improvement under the high temperature and pressure conditions. To the best of our knowledge, gFBT-g2T currently stands out as the sole single component conjugated polymer exhibiting stability after high pressure steam sterilization procedure aside from the composite PEDOT:PSS.[10–11]

To probe the reasons for the different stability profiles, we initially performed, differential scanning calorimetry (DSC) tests on gFBT-g2T and gFBT-3g2T. However, neither polymer exhibited any discernible melting nor crystallization peaks (Figure S10), despite X-ray scattering measurements indicating the presence of crystalline regions. This behavior is not unusual for conjugated polymers, which due to their rigid nature often exhibit melting temperature above their degradation and transitions with small enthalpy changes.[34] We therefore used a spectroscopic technique, which assesses changes in the UV–vis absorption spectrum following sequential thermal annealing by a deviation metric.[35] As illustrated in Figure 3e, a T_g can be estimated by the intersection of linear fits of the deviation metric. This suggests that the T_g of gFBT-3g2T (68 °C) is lower than gFBT-g2T (85 °C). Whilst this difference does not fully explain the different temperature stability observed, it is also noticeable that the deviation metric change for gFBT-3g2T was more pronounced. In contrast, the absorption

profile of gFBT-g2T showed negligible deviation metric variations around 100 °C. Thus, we conclude that the lower T_g of gFBT-3g2T is a contributory factor to the lower temperature stability observed.

To gain a more comprehensive understanding of the high performance and high temperature stability of gFBT-g2T, we conducted atomic force microscopy (AFM) measurements on films of gFBT-g2T and gFBT-3g2T. We compared the surface morphology changes in the polymer films under different conditions, including their pristine state, after thermal annealing in air and after the autoclave sterilization. As depicted in Figure 4a, the pristine films of both gFBT-g2T and gFBT-3g2T exhibited a very smooth surface with root mean square roughness (Rq) values of around 0.6 nm. However, the film surface of gFBT-g2T displayed a uniform and dense fibrous pattern, while gFBT-3g2T showed only some shallow patterns. After annealing in air for half an hour, the Rq value of gFBT-g2T (0.65 nm) were almost unchanged, and the fibrous pattern became finer. While, gFBT-3g2T showed a slight decrease in Rq value (0.47 nm) with no significant change in surface morphology. After autoclave sterilization, both films of gFBT-g2T and gFBT-3g2T underwent substantial changes, with the films becoming porous. As shown in Figure 4 and S22, gFBT-g2T formed randomly distributed pores of approximately 200–400 nm, which the majority of pores appearing circular. Voids also appeared in the gFBT-3g2T film, but they are less well-defined, with a larger distribution of sizes and non-circular shape. The roughness of both films increased, to Rq 3.19 nm and Rq = 3.41 nm, for gFBT-g2T and gFBT-3g2T respectively. The formation of such pores is reminiscent of the formation of porosity during the casting of films in high humidity, in which the condensation of water onto the cooling surface leads to droplet formation. Subsequent water evaporation leads to porous structures in a so-called 'breath figure' process.[36] Such as process has been observed during the spin-coating of conjugated polymer films, and has been correlated to improved OECT device performance.[25,37] Solvent vapour annealing has also been shown to lead to mesoporous polymers, via solvent swelling

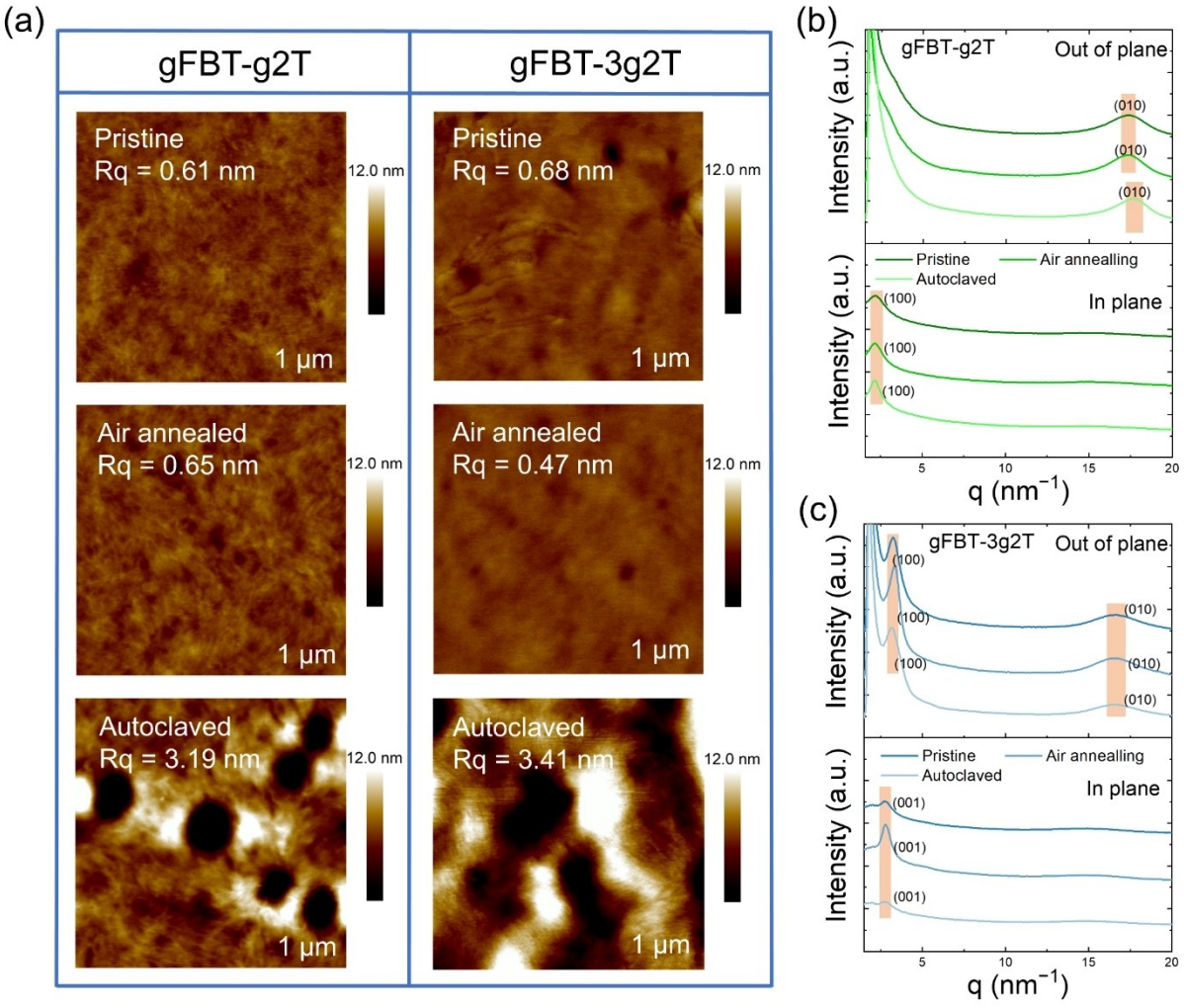

Figure 4. (a) AFM images of gFBT-g2T and gFBT-3g2T films in three states: pristine, annealed in air at 100 °C for 30 minutes and autoclaved, the image size is 1×1 micron. (b) Grazing incidence wide-angle X-ray scattering (GIWAXS) line-cut profiles of the gFBT-g2T and (c) gFBT-3g2T films in the in-plane and out-of-plane directions.

and subsequent phase separation through spinodal decomposition.[38] We believe a similar process is occurring in the current case, as the films are heated above T_g, swelling occurs via water absorption, followed by phase separation during extended annealing.

To analyze the microstructural features of the polymer films in the same three states, we collected the grazing incidence wide-angle X-ray scattering (GIWAXS) of the films (Figure 4b, c, Figure S23, S24 and Table S2). From the line-cut profiles of gFBT-g2T, it can be observed that the crystalline state of the pristine film and air-annealed film remained relatively unchanged. Scattering profiles suggested a face-on orientation, with broad out-of-plane (010) peaks at $q_z = 17.3\ nm^{-1}$ corresponding to a π–π stacking distance of 0.36 nm with diffraction peaks (100) at $q_{xy} = 2.19\ nm^{-1}$ corresponding to a d-spacing of 2.86 nm along the in-plane direction. In contrast, the film of gFBT-3g2T exhibited some changes in the solid-state microstructure between the pristine and the air-annealed films. Although the out-of-plane (100) and (010) peak positions remained constant, both at 3.24 and 16.6 nm^{-1} (corresponding to a d-spacing of 1.93 nm and a π–π stacking distance of 0.37 nm), the intensity of the (001) peak in the in-plane direction ($q_{xy} = 2.76\ nm^{-1}$, corresponding to a unit chain length of 2.27 nm) was increased after air annealing. The large lamellar d-spacing differences between the two polymers indicates that the intermolecular packing of gFBT-g2T is more disordered, which is more conducive to the interchain ions transport to some extent. After autoclave sterilization, gFBT-g2T showed no significant changes in the peak intensity, but showed a certain shift in the position of the out-of-plane (010) peak, with a $q_z = 17.7\ nm^{-1}$ corresponding to a π–π stacking distance of 0.35 nm. In the in-plane direction, the position and intensity of the (100) peak remain unchanged. The denser π–π stacking distance agrees with the enhanced performance after the autoclave sterilization process. Meanwhile, gFBT-3g2T didn't exhibit significant changes after autoclaving.

To further investigate the effects of ion doping and de-doping on the crystalline state of the films, we conducted GIWAXS tests on the pristine, doped, and de-doped states films of gFBT-g2T and gFBT-3g2T (Figure S25, S26 and Table S3). For the gFBT-g2T film, the electrochemical doping and de-doping processes did not affect the in-plane direction stacking, with the lamellar diffraction peak (100) unchanged. In the out-of-plane direction, a new (001) peak appeared after electrochemical doping, while the π–π (010) peak remained unchanged. Following further electrochemical de-doping process of the film, the new (001) peak disappeared, and the (010) peak showed only a slight decrease in intensity, indicating the electrochemical doping and de-doping processes did not affect the crystalline regions of gFBT-g2T. For the gFBT-3g2T film, in the in-plane direction, the (001) peak disappeared after doping and reappeared after the de-doping process, but with significantly reduced intensity. In the out-of-plane direction, after doping, the intensities of both the (100) peak and π–π (010) peak decreased. Following electrochemical de-doping, the (010) peak almost vanished, suggesting significant changes of the crystalline regions of the gFBT-3g2T film. These observations support the observation that gFBT-g2T is more stable than gFBT-3g2T during the electrochemical doping and de-doping processes.

Conclusion

We presented a series of novel D-A polymers prepared with an easily accessible synthesis route. We systematically studied the polymers' photophysical, electrochemical, and morphological properties along with molecular packing and electron transport behavior by optical spectroscopy, cyclic voltammetry, atomic force microscopy, and GIWAXS techniques. Introducing alkoxy side chains in the donor unit reduced the ionisation potential, and significantly enhanced the polymer's ion transport capability, making them more susceptible to doping. The transition from gFBT-2T to gFBT-g2T resulted in a three-order-of-magnitude increase in OECTs performance yielding a $g_{m,norm}$ of 298 (± 10.4) $S\,cm^{-1}$, with a corresponding μC^* of 847 $F\,V^{-1}\,cm^{-1}\,s^{-1}$, due to the high μ of 5.76 $cm^2\,V^{-1}\,s^{-1}$. These values are among the highest among D-A polymer materials reported to date for accumulation mode devices. In contrast, gFBT-3g2T with longer side chains in the donor unit, exhibited a $g_{m,norm}$ of $43.5 \pm 1.4\ S\,cm^{-1}$ and a μC^* of 202 $F\,V^{-1}\,cm^{-1}\,s^{-1}$, attributed to its lower ion-electron coupled transport capability. More importantly, gFBT-g2T exhibited exceptional high temperature stability, which not only maintained the device current and transconductance after high temperature annealing in nitrogen but also retained 84 % of the initial saturated current and transconductance after half an hour of air annealing. Impressively, immersing the gFBT-g2T OECTs in boiling water for half an hour results to only 2 % reduction of the initial channel current and approx 6 % drop in its transconductance. After undergoing a standard autoclave steam sterilization procedure for 20 minutes, the films became porous and the device not only maintained high current and transconductance but also showed a slight improvement. We believe that gFBT-g2T is a promising p-type semiconductor for accumulation mode OECTs with potential for reliable and safe use in implantable bioelectronics among numerous other medical applications.

Acknowledgements

We would like to thank the Engineering and Physics Science Research Council (EPSRC) (EP/V048686/1 and EP/T028513/1), the Royal Society and Wolfson Foundation, and the King Abdullah University of Science and Technology (KAUST) Office of Sponsored Research (OSR) under Award No. OSR-2020-CRG8-4095 for financial support.

Conflict of Interest

The authors declare no conflict of interest.

Data Availability Statement

The data that support the findings of this study are available from the corresponding author upon reasonable request.

Keywords: organic electrochemical transistors · high temperature stability · autoclave · mixed ionic electronic conductors · donor-acceptor polymers

[1] a) N. A. Kukhta, A. Marks, C. K. Luscombe, *Chem. Rev.* **2022**, *122*, 4325–4355; b) A. Nawaz, Q. Liu, W. L. Leong, K. E. Fairfull-Smith, P. Sonar, *Adv. Mater.* **2021**, *33*, e2101874; c) D. T. Simon, E. O. Gabrielsson, K. Tybrandt, M. Berggren, *Chem. Rev.* **2016**, *116*, 13009–13041; d) P. C. Harikesh, C. Y. Yang, H. Y. Wu, S. Zhang, M. J. Donahue, A. S. Caravaca, J. D. Huang, P. S. Olofsson, M. Berggren, D. Tu, S. Fabiano, *Nat. Mater.* **2023**, *22*, 242–248; e) G. Gao, J. H. Chen, M. J. Jing, J. Hu, Q. Xu, C. S. Wang, H. Zhou, P. Lin, G. Chen, W. W. Zhao, *Adv. Funct. Mater.* **2023**, *33*, 2300580; f) H. Kim, Y. Won, H. W. Song, Y. Kwon, M. Jun, J. H. Oh, *Adv. Sci.* **2024**, *11*, e2306191.

[2] a) J. Rivnay, S. Inal, A. Salleo, R. M. Owens, M. Berggren, G. G. Malliaras, *Nat. Rev. Mater.* **2018**, *3*, 17086; b) H. Shen, A. Abtahi, B. Lussem, B. W. Boudouris, J. Mei, *ACS Appl. Electron. Mater.* **2021**, *3*, 2434–2448; c) H. Sun, M. Vagin, S. Wang, X. Crispin, R. Forchheimer, M. Berggren, S. Fabiano, *Adv. Mater.* **2018**, *30*, 1704986; d) A. F. Paterson, A. Savva, S. Wustoni, L. Tsetseris, B. D. Paulsen, H. Faber, A. H. Emwas, X. Chen, G. Nikiforidis, T. C. Hidalgo, M. Moser, I. P. Maria, J. Rivnay, I. McCulloch, T. D. Anthopoulos, S. Inal, *Nat. Commun.* **2020**, *11*, 3004.

[3] B. D. Paulsen, K. Tybrandt, E. Stavrinidou, J. Rivnay, *Nat. Mater.* **2020**, *19*, 13–26.

[4] A. Marks, S. Griggs, N. Gasparini, M. Moser, *Adv. Mater. Interfaces* **2022**, *9*, 2102039.

[5] J. Song, H. Liu, Z. Zhao, P. Lin, F. Yan, *Adv. Mater.* **2023**, e2300034.

[6] P. Alarcon-Espejo, R. Sarabia-Riquelme, G. M. Matrone, M. Shahi, S. Mahmoudi, G. S. Rupasinghe, V. N. Le, A. M. Mantica, D. Qian, T. J. Balk, J. Rivnay, M. Weisenberger, A. F. Paterson, *Adv. Mater.* **2023**, e2305371.

[7] a) E. Bihar, Y. Deng, T. Miyake, M. Saadaoui, G. G. Malliaras, M. Rolandi, *Sci. Rep.* **2016**, *6*, 27582; b) M. Y. Lee, H. R. Lee, C. H. Park, S. G. Han, J. H. Oh, *Acc. Chem. Res.* **2018**, *51*, 2829–2838.

[8] X. Wu, J. Feng, J. Deng, Z. Cui, L. Wang, S. Xie, C. Chen, C. Tang, Z. Han, H. Yu, X. Sun, H. Peng, *Science China Chemistry* **2020**, *63*, 1281–1288.

[9] a) S. Han, S. Yu, S. Hu, H.-j. Chen, J. Wu, C. Liu, *J. Mater. Chem. C* **2021**, *9*, 11801–11808; b) X. Wu, S. Chen, M. Moser, A. Moudgil, S. Griggs, A. Marks, T. Li, I. McCulloch, W. L. Leong, *Adv. Funct. Mater.* **2022**, *33*, 2209354; c) S. Zhang, P. Ding, T. P. Ruoko, R. Wu, M. A. Stoeckel, M. Massetti, T. Liu, M. Vagin, D. Meli, R. Kroon, J. Rivnay, S. Fabiano, *Adv. Funct. Mater.* **2023**, *33*, 2302249.

[10] I. Uguz, M. Ganji, A. Hama, A. Tanaka, S. Inal, A. Youssef, R. M. Owens, P. P. Quilichini, A. Ghestem, C. Bernard, S. A. Dayeh, G. G. Malliaras, *Adv. Healthcare Mater.* **2016**, *5*, 3094–3098.

[11] S. M. Kim, C. H. Kim, Y. Kim, N. Kim, W. J. Lee, E. H. Lee, D. Kim, S. Park, K. Lee, J. Rivnay, M. H. Yoon, *Nat. Commun.* **2018**, *9*, 3858.

[12] a) B. Ding, I. Y. Jo, H. Yu, J. H. Kim, A. V. Marsh, E. Gutierrez-Fernandez, N. Ramos, C. L. Rapley, M. Rimmele, Q. He, J. Martin, N. Gasparini, J. Nelson, M. H. Yoon, M. Heeney, *Chem. Mater.* **2023**, *35*, 3290–3299; b) M. Moser, T. C. Hidalgo, J. Surgailis, J. Gladisch, S. Ghosh, R. Sheelamanthula, Q. Thiburce, A. Giovannitti, A. Salleo, N. Gasparini, A. Wadsworth, I. Zozoulenko, M. Berggren, E. Stavrinidou, S. Inal, I. McCulloch, *Adv. Mater.* **2020**, *32*, e2002748.

[13] a) J. D. Yuen, F. Wudl, *Energy Environ. Sci.* **2013**, *6*, 392; b) J. Qi, J. Han, X. Zhou, D. Yang, J. Zhang, W. Qiao, D. Ma, Z. Y. Wang, *Macromolecules* **2015**, *48*, 3941–3948; c) S. Holliday, Y. Li, C. K. Luscombe, *Prog. Polym. Sci.* **2017**, *70*, 34–51.

[14] a) M. Moser, A. Savva, K. Thorley, B. D. Paulsen, T. C. Hidalgo, D. Ohayon, H. Chen, A. Giovannitti, A. Marks, N. Gasparini, A. Wadsworth, J. Rivnay, S. Inal, I. McCulloch, *Angew. Chem. Int. Ed. Engl.* **2021**, *60*, 7777–7785; b) I. Y. Jo, D. Jeong, Y. Moon, D. Lee, S. Lee, J. G. Choi, D. Nam, J. H. Kim, J. Cho, S. Cho, D. Y. Kim, H. Ahn, B. J. Kim, M. H. Yoon, *Adv. Mater.* **2023**, e2307402; c) K. Feng, W. Shan, S. Ma, Z. Wu, J. Chen, H. Guo, B. Liu, J. Wang, B. Li, H. Y. Woo, S. Fabiano, W. Huang, X. Guo, *Angew. Chem. Int. Ed. Engl.* **2021**, *60*, 24198–24205; d) W. Yang, K. Feng, S. Ma, B. Liu, Y. Wang, R. Ding, S. Y. Jeong, H. Y. Woo, P. K. L. Chan, X. Guo, *Adv. Mater.* **2024**, *36*, e2305416; e) K. Feng, W. Shan, J. Wang, J. W. Lee, W. Yang, W. Wu, Y. Wang, B. J. Kim, X. Guo, H. Guo, *Adv. Mater.* **2022**, *34*, e2201340; f) J. Kimpel, Y. Kim, J. Asatryan, J. Martin, R. Kroon, C. Muller, *Chem. Sci.* **2024**, *15*, 7679–7688.

[15] a) A. Giovannitti, R. B. Rashid, Q. Thiburce, B. D. Paulsen, C. Cendra, K. Thorley, D. Moia, J. T. Mefford, D. Hanifi, D. Weiyuan, M. Moser, A. Salleo, J. Nelson, I. McCulloch, J. Rivnay, *Adv. Mater.* **2020**, *32*, e1908047; b) A. Savva, C. Cendra, A. Giugni, B. Torre, J. Surgailis, D. Ohayon, A. Giovannitti, I. McCulloch, E. Di Fabrizio, A. Salleo, J. Rivnay, S. Inal, *Chem. Mater.* **2019**, *31*, 927–937.

[16] M. Moser, L. R. Savagian, A. Savva, M. Matta, J. F. Ponder, T. C. Hidalgo, D. Ohayon, R. Hallani, M. Reisjalali, A. Troisi, A. Wadsworth, J. R. Reynolds, S. Inal, I. McCulloch, *Chem. Mater.* **2020**, *32*, 6618–6628.

[17] T. C. Parker, D. G. Patel, K. Moudgil, S. Barlow, C. Risko, J.-L. Brédas, J. R. Reynolds, S. R. Marder, *Mater. Horiz.* **2015**, *2*, 22–36.

[18] a) B. Ding, G. Kim, Y. Kim, F. D. Eisner, E. Gutierrez-Fernandez, J. Martin, M. H. Yoon, M. Heeney, *Angew. Chem. Int. Ed. Engl.* **2021**, *60*, 19679–19684; b) S. Cong, J. Chen, B. Ding, L. Lan, Y. Wang, C. Chen, Z. Li, M. Heeney, W. Yue, *Mater. Horiz.* **2023**, *10*, 3090–3100.

[19] R. K. Hallani, B. D. Paulsen, A. J. Petty, 2nd, R. Sheelamanthula, M. Moser, K. J. Thorley, W. Sohn, R. B. Rashid, A. Savva, S. Moro, J. P. Parker, O. Drury, M. Alsufyani, M. Neophytou, J. Kosco, S. Inal, G. Costantini, J. Rivnay, I. McCulloch, *J. Am. Chem. Soc.* **2021**, *143*, 11007–11018.

[20] M. Rimmele, Z. Qiao, J. Panidi, F. Furlan, C. Lee, W. L. Tan, C. R. McNeill, Y. Kim, N. Gasparini, M. Heeney, *Mater. Horiz.* **2023**, *10*, 4202–4212.

[21] H. Jia, Z. Huang, P. Li, S. Zhang, Y. Wang, J.-Y. Wang, X. Gu, T. Lei, *J. Mater. Chem. C* **2021**, *9*, 4927–4934.

[22] a) R. Halaksa, J. H. Kim, K. J. Thorley, P. A. Gilhooly-Finn, H. Ahn, A. Savva, M. H. Yoon, C. B. Nielsen, *Angew. Chem. Int. Ed. Engl.* **2023**, *62*, e202304390; b) J. H. Kim, R. Halaksa, I. Y. Jo, H. Ahn, P. A. Gilhooly-Finn, I. Lee, S. Park, C. B. Nielsen, M. H. Yoon, *Nat. Commun.* **2023**, *14*, 7577.

[23] S. Griggs, A. Marks, D. Meli, G. Rebetez, O. Bardagot, B. D. Paulsen, H. Chen, K. Weaver, M. I. Nugraha, E. A. Schafer, J. Tropp, C. M. Aitchison, T. D. Anthopoulos, N. Banerji, J. Rivnay, I. McCulloch, *Nat. Commun.* **2022**, *13*, 7964.

[24] S. Chapi, *J. Science: Advanced Materials and Devices* **2020**, *5*, 322–329.

[25] L. Lan, J. Chen, Y. Wang, P. Li, Y. Yu, G. Zhu, Z. Li, T. Lei, W. Yue, I. McCulloch, *Chem. Mater.* **2022**, *34*, 1666–1676.

[26] I. Zozoulenko, A. Singh, S. K. Singh, V. Gueskine, X. Crispin, M. Berggren, *ACS Appl. Polym. Mater.* **2018**, *1*, 83–94.
[27] S. Lin, P. M. Usov, A. J. Morris, *Chem. Commun.* **2018**, *54*, 6965–6974.
[28] Y. Wang, A. Koklu, Y. Zhong, T. Chang, K. Guo, C. Zhao, T. C. H. Castillo, Z. Bu, C. Xiao, W. Yue, W. Ma, S. Inal, *Adv. Funct. Mater.* **2023**, *34*, 2304103.
[29] A. Giovannitti, D. T. Sbircea, S. Inal, C. B. Nielsen, E. Bandiello, D. A. Hanifi, M. Sessolo, G. G. Malliaras, I. McCulloch, J. Rivnay, *Proc. Natl. Acad. Sci. USA* **2016**, *113*, 12017–12022.
[30] A. Savva, R. Hallani, C. Cendra, J. Surgailis, T. C. Hidalgo, S. Wustoni, R. Sheelamanthula, X. Chen, M. Kirkus, A. Giovannitti, A. Salleo, I. McCulloch, S. Inal, *Adv. Funct. Mater.* **2020**, *30*, 1907657.
[31] H. Liao, J. Chen, L. Lan, Y. Yu, G. Zhu, J. Duan, X. Zhu, H. Dai, M. Xiao, Z. Li, W. Yue, I. McCulloch, *ACS Appl. Mater. Interfaces* **2022**, *14*, 16477–16486.
[32] K. Kuribara, H. Wang, N. Uchiyama, K. Fukuda, T. Yokota, U. Zschieschang, C. Jaye, D. Fischer, H. Klauk, T. Yamamoto, K. Takimiya, M. Ikeda, H. Kuwabara, T. Sekitani, Y. L. Loo, T. Someya, *Nat. Commun.* **2012**, *3*, 723.
[33] Y. Wang, E. Zeglio, H. Liao, J. Xu, F. Liu, Z. Li, I. P. Maria, D. Mawad, A. Herland, I. McCulloch, W. Yue, *Chem. Mater.* **2019**, *31*, 9797–9806.
[34] C. Müller, *Chem. Mater.* **2015**, *27*, 2740–2754.
[35] S. E. Root, M. A. Alkhadra, D. Rodriquez, A. D. Printz, D. J. Lipomi, *Chem. Mater.* **2017**, *29*, 2646–2654.
[36] A. Zhang, H. Bai, L. Li, *Chem. Rev.* **2015**, *115*, 9801–9868.
[37] L. Huang, Z. Wang, J. Chen, B. Wang, Y. Chen, W. Huang, L. Chi, T. J. Marks, A. Facchetti, *Adv. Mater.* **2021**, *33*, e2007041.
[38] M. R. Krishnan, Y. C. Chien, C. F. Cheng, R. M. Ho, *Langmuir* **2017**, *33*, 8428–8435.

Manuscript received: August 25, 2024
Accepted manuscript online: September 18, 2024
Version of record online: November 2, 2024